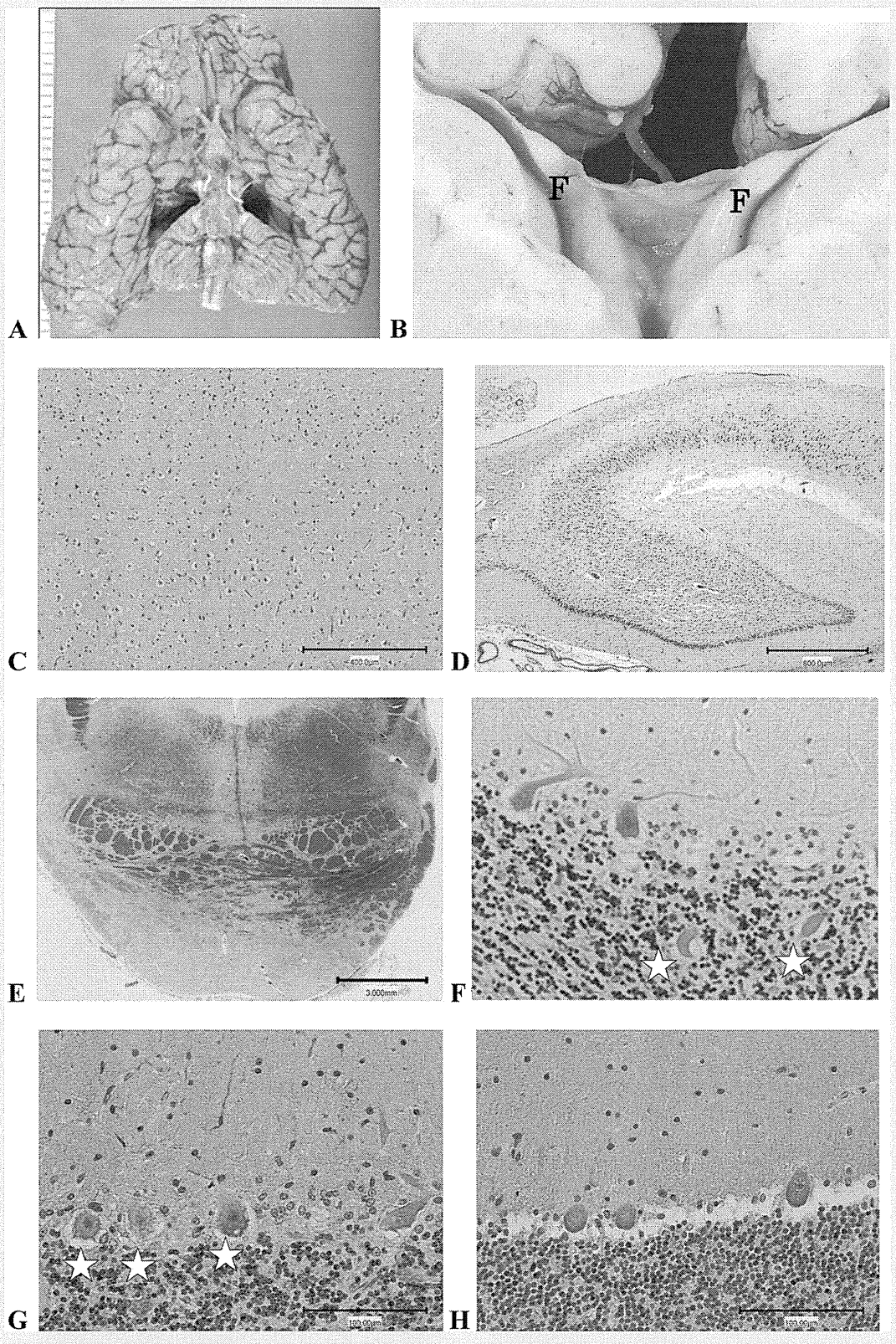

FIG. 1. A: The cerebrum was small, and both the cerebellum and brainstem were severely hypoplastic. B: The cross section of the brain showed absence of corpus callosum, in which fornix (F) was identified. C: The superior frontal cortex had preservation of neurons, bar = 400 μm. D: In the hippocampus, neurons were spared, bar = 800 μm. E: In the pontine base, the pyramidal tract was hypoplastic, bar = 3 mm. F: The formation of torpedo (stars) was found in the inner granule layer. G, H: Immunoreactivity for LC3 in most of the Purkinje cells was reduced in the case (G, stars), whereas that was spared in the control (H), bars = 100 μm.

cerebellar hemispheres, and tonsil (F). Dendrite swelling of the Purkinje cells was found to a lesser extent. Immunohistochemistry on autophagy was done in the frontal and temporal cortex, the basal ganglia, and the cerebellar cortex in the control and case. Immunoreactivity for LC3 was reduced in some of the remaining Purkinje cells in the patient (G), whereas the Purkinje cells in the control were immunoreactive for LC3 uniformly (H). There were no changes in immunohistochemistry for either LC3 or p62 in other brain regions.

The previous autopsy report stressed the vacuole formation in the heart, which was also seen in our case. In the brain, mild polymicrogyria in the occipital cortex, and Purkinje cell agenesis with granule cell loss were reported [Rogers et al., 2011]. On the other hand, our case did not show dysplastic changes in the cerebrum, although he demonstrated those in the pyramidal tract. The Purkinje cells and the granule cells were comparatively well preserved. Nevertheless, axonal and dendrite swellings were predominant in the Purkinje cells. Such changes have been reported in the cerebellar cortex with metabolic errors and toxic disorders such as Menkes disease, mitochondrial encephalopathy, congenital disorders of glycosylation, and organic mercury intoxication [Takahashi et al., 2005], and neurodegenerative disorders [Matsumoto et al., 1998]. Accordingly, the presence of axonal and dendrite swellings may reflect disturbed metabolism and/or latent degeneration in the cerebellar cortex. During autophagy, cytosolic LC3 forms a LC3-phosphatidylethanolamine conjugate, which is recruited to autophagosomal membranes [Tanida et al., 2008], and phosphorylation of p62 is involved in degeneration associated with selective autophagy [Ichimura et al., 2013]. Since autophagosomal clearance associated with *EPG-5* was impaired in Vici syndrome, the p62-immunoreactivity in the cardiac muscle and the reduced immunoreactivity for LC3 in the Purkinje cells may be involved in the vacuole formation in the heart, and the axonal and dendrite swellings in the Purkinje cells, respectively. Vici syndrome was originally considered a malformation syndrome. However, it is likely that the genetically defined disturbance in autophagy causes degenerative organ changes, in addition to malformations.

REFERENCES

Cullup T, Kho AL, Dionisi-Vici C, Brandmeier B, Smith F, Urry Z, Simpson MA, Yau S, Bertini E, McClelland V, Al-Owain M, Koelker S, Koerner C, Hoffmann GF, Wijburg FA, ten Hoedt AE, Rogers RC, Manchester D, Miyata R, Hayashi M, Said E, Soler D, Kroisel PM, Windpassinger C, Filloux FM, Al-Kaabi S, Hertecant J, Del Campo M, Buk S, Bodi I, Goebel HH, Sewry CA, Abbs S, Mohammed S, Josifova D, Gautel M, Jungbluth H. 2013. Recessive mutations in DPG-5 cause Vici syndrome, a multisystem disorder with defective autophagy. Nat Genet 45:83–87.

del Campo M, Hall BD, Aeby A, Nassogne MC, Verloes A, Roche C, Gonzalez C, Sanchez H, Garcia-Alix A, Cabanas F, Escudero RM, Hernandez R, Quero J. 1999. Albinism and agenesis of the corpus callosum with profound developmental delay: Vici syndrome, evidence for autosomal recessive inheritance. Am J Med Genet 85:479–485.

Ichimura Y, Waguri S, Sou YS, Kageyama S, Hasegawa J, Ishimura R, Saito T, Yang Y, Kouno T, Fukutomi T, Hoshii T, Hirao A, Takagi K, Mizushima T, Motohashi H, Lee MS, Yoshimori T, Tanaka K, Yamamoto M, Komatsu M. 2013. Phosphorylation of p62 activates the Keap1-Nrf2 pathway during selective autophagy. Mol Cell 51:618–631.

Matsumoto R, Nakano I, Arai N, Oda M, Yagishita S, Hashizume Y. 1998. Loss of the dentate nucleus neurons is associated with torpedo formation: A morphometric study in progressive supranuclear palsy and dentatorubro-pallidoluysian atrophy. Acta Neuropathol 95:149–153.

Miyata R, Hayashi M, Sato H, Sugawara Y, Yui T, Araki S, Hasegawa T, Doi S, Kohyama J. 2007. Sibling cases of Vici syndrome: Sleep abnormalities and complications with renal tubular acidosis. Am J Med Genet Part A 143A:189–194.

Rogers RC, Aufmuth B, Monesson S. 2011. Vici syndrome: A rare autosomal recessive syndrome with brain anomalies cardiomyopathy, and severe intellectual disability. Case Rep Genet 2011:421582.

Takahashi T, Arai N, Shimamura M, Suzuki Y, Yamashita S, Iwamoto H, Inayama Y, Kameda Y, Kuroiwa Y. 2005. Autopsy case of acute encephalopathy linked to familial hemiplegic migraine with cerebellar atrophy and mental retardation. Neuropathology 25:228–234.

Tanida I, Ueno T, Kominami E. 2008. LC3 and autophagy. Methods Mol Biol 445:77–88.

Vici CD, Sabetta G, Gambarara M, Vigevano F, Bertini E, Boldrini R, Parisi SG, Quinti I, Aiuti F, Fiorilli M. 1988. Agenesis of the corpus callosum, combined immunodeficiency, bilateral cataract, and hypopigmentation in two brothers. Am J Med Genet 29:1–8.

Biomedical Research (Tokyo) **35** (4) 227-236, 2014

A novel approach to the histological diagnosis of pediatric nephrotic syndrome by low vacuum scanning electron microscopy

Shinichi OKADA[1], Sumire INAGA[2], Yasuo KAWABA[1], Takuya HANADA[1], Atsushi HAYASHI[1], Hironobu NAKANE[2], Tomonori NAGURO[2], Toshiyuki KAIDOH[2], and Susumu KANZAKI[1]

[1] Division of Pediatrics and Perinatology and [2] Department of Anatomy, Faculty of Medicine, Tottori University

(Received 21 April 2014; and accepted 6 May 2014)

ABSTRACT

Despite intensive treatment, steroid-resistant nephrotic syndrome (NS) often progresses to end-stage renal disease. Therefore, a more accurate and quick histological diagnosis is required to properly treat such patients. The aim of this study was to introduce a novel approach to the histological diagnosis of pediatric NS by low vacuum scanning electron microscopy (LVSEM) and to describe the morphological differences in glomeruli between steroid-sensitive and steroid-resistant NS specimens. The subjects were three patients with steroid-sensitive NS and four patients with steroid-resistant NS. Conventional renal biopsy paraffin sections were stained with platinum-blue (Pt-blue) or periodic acid methenamine silver (PAM) and directly observed under LVSEM at magnifications between ×50 and ×10,000. The Pt-blue-stained sections showed three-dimensional structural alterations in glomerular podocytes and foot processes. PAM-stained sections showed changes in the structure and thickness of the glomerular basement membrane (GBM). Consequently, many round-shaped podocytes and elongated primary foot processes were exclusively recognized in steroid-resistant NS, although irregularities in foot process interdigitation, fusions, effacements, and microvillus transformations were observed in both steroid-sensitive and steroid-resistant NS. Irregularities in thickness and the wrinkling of GBMs were clearly detected in steroid-resistant NS. The evaluation by LVSEM is probably useful for the renal histological diagnosis of pediatric NS.

Nephrotic syndrome (NS) comprises proteinuria, hypoalbuminemia, hypercholesterolemia, and edema. Pediatric patients with NS are usually treated with corticosteroids (13). Patients who respond to steroids (steroid-sensitive NS) have good clinical outcomes, whereas patients who do not respond to steroids (steroid-resistant NS) are predisposed to the development of end-stage renal disease. Histopathologically, most pediatric patients with steroid-sensitive NS show minor glomerular abnormalities, and patients with steroid-resistant NS generally have focal segmental glomerulosclerosis (FSGS) (25). Under light microscopy (LM), minor glomerular abnormalities are defined as a slight or no increase in the mesangial matrix or cellularity without focal segmental glomerular collapse, scarring, endocapillary proliferation, or adhesions. FSGS shows focal and segmental glomerular collapse, scarring, endocapillary proliferation, or adhesions of glomeruli with minimal abnormalities (21). However, it is not clear whether the glomeruli with no obvious changes in FSGS are different from those in minor glomerular abnormalities. In addition, it is difficult to diagnose FSGS when the NS biopsy section does not include glomeruli with the typical alterations of FSGS described above, although the differential diagnosis between minor glomerular abnormalities and FSGS is very

Address correspondence to: Shinichi Okada, MD, PhD
Division of Pediatrics and Perinatology, Faculty of Medicine, Tottori University, 36-1 Nishi-cho, Yonago City, Tottori, Japan
Tel: +81-859-38-6557, Fax: +81-859-38-6559
E-mail: sokada@med.tottori-u.ac.jp

important in pediatric cases of NS.

The typical renal histological findings of NS by transmission electron microscopy (TEM) and scanning electron microscopy (SEM) are podocyte foot process fusions, effacements, and microvillus transformations (23), although these features cannot be elucidated under LM due to resolution limitations. TEM is superior to investigate cross-sectional images not only of podocytes but also of other components in glomeruli; however, performing three-dimensional and whole-wide observations using ultra-thin sections is difficult due to the limitation of the observable size. Therefore, with TEM, focal glomerular abnormalities may be missed in some cases. SEM is suitable for the three-dimensional observation of surface alterations of podocytes as processing is easier and shorter with SEM than with TEM (1, 2, 11, 16, 19, 24, 28). In addition, SEM of acellular glomeruli in human glomerulonephritis was developed to visualize the surface structure of the glomerular basement membrane (GBM) that is present between podocytes and endothelial cells (4, 6). Using this technique, some researchers have investigated GBM alterations and gap formations in a three-dimensional manner (5, 7, 8, 20, 26). Despite such advantages, however, conventional SEM is not currently utilized for the pathological diagnosis of renal biopsy specimens, because dedicated preparation techniques and equipment are required. On the other hand, Phillips *et al.* (22) reviewed new methodologies such as two-photon microscopy that optimize three-dimensional, multicolor imaging and single-cell segmentation of glomerular components in renal biopsy specimens to facilitate exploration of glomeruli.

We previously demonstrated the usefulness of low vacuum scanning electron microscopy (LVSEM) for the rapid three-dimensional analysis of renal biopsy samples by using conventional paraffin sections to evaluate the histological findings of glomeruli (9, 17). Vacuum condition is set at tens to hundreds Pa in the LVSEM chamber, although it is 10^{-3} Pa or higher in the conventional SEM. The advantages of the LVSEM approach include the ability to easily conduct overviews of whole renal paraffin sections at low magnifications typical of LM observations and detailed three-dimensional analysis of every glomerulus in a section with a high resolution close to that of TEM. The observable area of a biopsy sample is not limited under LVSEM, unlike with conventional TEM. Accordingly, LVSEM allows detailed and efficient three-dimensional whole-wide observation of renal biopsy specimens more easily than LM, TEM, or conventional SEM. In the backscattered electron (BSE) mode of LVSEM, glomerular components such as podocytes, endothelium, mesangium, and GBM can be distinguished and investigated by staining with platinum-blue (Pt-blue) or periodic acid methenamine silver (PAM), because both stains contain a heavy metal salt for enhancing the BSE signal (10). Both the surface and the subsurface structures of renal glomeruli can be observed with a high resolution of up to ×10,000 (9).

In the present study, we introduce a novel approach to the histological diagnosis of pediatric NS by LVSEM and describe the three-dimensional morphological findings of glomeruli in pediatric steroid-sensitive NS and steroid-resistant NS, especially podocytes, foot processes, and GBM.

MATERIALS AND METHODS

We used renal biopsy tissue samples obtained from seven pediatric NS patients (three steroid-sensitive NS cases and four steroid-resistant NS cases) that had been already diagnosed at Tottori University Hospital as minor glomerular abnormalities or FSGS, under the approval of the Ethics Committee of Tottori University (Permission No. 1093). The samples were prepared using paraffin sections for the LVSEM, introduced by Inaga *et al.* (9), and the conventional TEM method.

Tissue preparation and light microscopy. The renal biopsy tissue samples were fixed with a 10% neutral buffered formalin solution and embedded in paraffin, using the standard method. Each paraffin block was cut into thin sections (5–10 μm) and mounted on standard-sized glass slides (76 mm × 26 mm). The sections on the slides were deparaffinized with xylol and transferred to distilled water after passing through a graded alcohol series. After deparaffinization, some of the renal sections were stained with hematoxylin and eosin (HE) and periodic acid-Schiff (PAS), using the conventional staining method for LM observation.

Low vacuum scanning electron microscopy. The deparaffinized renal sections in each case were stained with Pt-blue to observe the surface structure of glomeruli or with PAM to observe GBMs. A Pt-blue aqueous solution was adjusted to pH 9 (TI-blue staining kit: Nisshin EM Co. Ltd., Tokyo, Japan) and placed on the renal sections for 10–15 min at room temperature. After washing with distilled water for 1–2 min, renal sections on the slides were observed

by LVSEM without cover slips. Some of the Pt-blue-stained sections were coated with platinum in an ion sputter (E-1030; Hitachi Co. Ltd., Tokyo, Japan) to observe the surface structure of podocyte foot processes more clearly, after the first LVSEM observation. PAM staining was performed using the conventional method for LM observation without the final HE staining process. The stained sections on the slides were directly observed and photographed with LVSEM (Hitachi Miniscope TM-1000 and TM3000; Hitachi Co., Ltd., Tokyo) at 30 Pa and an acceleration voltage of 15 kV, using the charge-up reduction BSE mode.

Transmission electron microscopy. We prepared ultrathin epoxy resin sections of several biopsy samples obtained from the same steroid-sensitive NS and steroid-resistant NS cases using the conventional method. They were fixed with a 2.5% glutaraldehyde solution and a 1% OsO_4 solution, embedded in epoxy resin, ultrathin sectioned, stained with uranyl acetate and lead citrate, and observed under TEM (Hitachi H-7100; Hitachi Co., Ltd.) at an acceleration voltage of 70 kV.

RESULTS

We observed the morphological alterations of glomeruli in renal biopsy sections of pediatric patients with steroid-sensitive NS and steroid-resistant NS under LM, LVSEM, and TEM. Figure 1 shows LM images of glomeruli from steroid-sensitive NS (Fig. 1a) and steroid-resistant NS (Fig. 1b) specimens stained with PAS. Glomeruli in both specimens showed similar findings with regard to minor glomerular abnormalities. This steroid-resistant NS specimen showed no FSGS. Figure 2 shows LVSEM images of two serial biopsy sections of steroid-sensitive NS specimens stained with Pt-blue (Fig. 2a) or PAM (Fig. 2c) observed at low magnification (×50). All glomeruli in each section could be observed in a broad range of specimens. Each glomerulus appeared as a different image due to variations in BSE signal brightness that depended on the stain. A complete sectioned renal glomerulus is shown at a magnification of approximately ×1,000 under LVSEM (Fig. 2b, d). The cellular constituents of glomeruli were well distinguished by staining with Pt-blue (Fig. 2b), whereas the GBM and the mesangial matrix were distinctly detectable with PAM staining (Fig. 2d). Every glomeruli component, especially podocytes, endothelial cells, and GBM, was investigated at higher magnifications of up to ×10,000. Figures 3 and 4 show three-dimensional images of Pt-blue-stained glomeruli in steroid-sensitive NS and steroid-resistant NS, respectively. The cut surface view of a glomerulus in steroid-sensitive NS showed no hypercellularity, and the glomerular capillary lumens were fully patent (Fig. 2b, 3a). Podocytes, endothelial cells, and mesangial cells appeared bright, whereas the GBM and mesangial matrix appeared dark. In Bowman's space, surface structures of podocytes and the interdigitation of foot processes were observed three-dimensionally (Fig. 3a–d). Podocytes from surface views had normal alignments of primary and secondary foot processes, but had disruptions of interdigitation of foot processes in part. Irregular width of secondary foot processes of podocytes, shortening changes of foot processes, and unclear margins of each secondary foot process

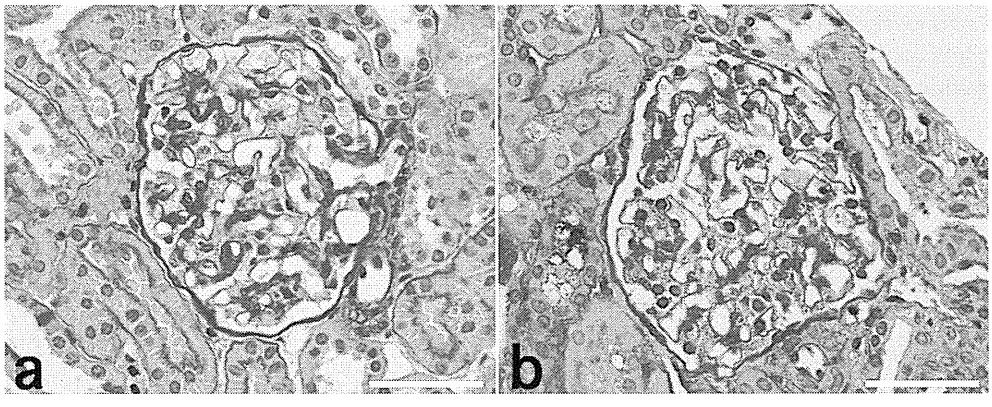

Fig. 1 Light microscopy images of renal glomeruli stained with PAS in steroid-sensitive NS (a) and steroid-resistant NS (b) specimens with a direct magnification of ×400. There were no significant pathological findings in glomeruli with minor abnormalities from both specimens. The section observed in this case of steroid-resistant NS (b) shows no focal segmental glomerulosclerosis. Bars: 50 μm

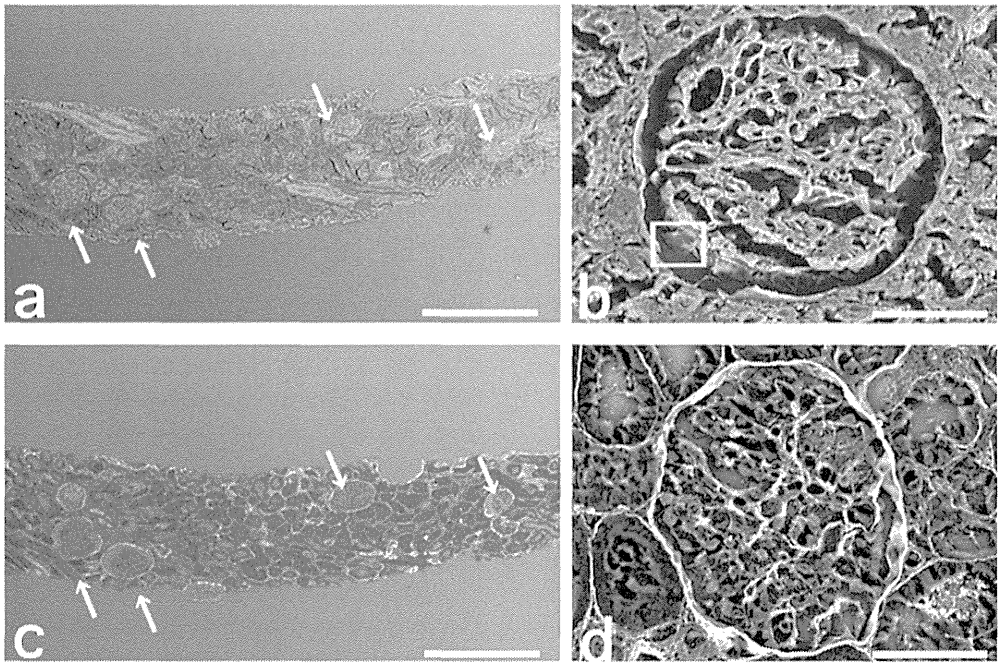

Fig. 2 Low vacuum scanning electron microscopy (LVSEM) images of renal biopsy paraffin sections in steroid-sensitive NS. Comparative LVSEM images of serial sections between Pt-blue-stained (a, b) and PAM-stained specimen (c, d). Many of the glomeruli (arrows) can be observed in each section at a low magnification (×50) (a, c). At a higher magnification (×1,000), the entire glomerulus structure is clearly observed in the Pt-blue-stained specimen (b), and the GBM and the mesangial matrix are identified in the sections stained with PAM (d). A part of glomerular surface within a square shown in (b) is magnified in Fig. 3c. Bars: 500 μm (a, c), 50 μm (b, d)

were visible (Fig. 3d).

Figure 4 shows LVSEM images of Pt-blue-stained glomeruli in steroid-resistant NS. We observed a three-dimensional overview of the surface structure of glomeruli in this specimen. The microvillus transformation of podocytes and the round-shaped podocyte cell bodies were recognized in wide range at a magnification of ×1,000 (Fig. 4a). Observation at a higher magnification clearly showed the surface structures of podocytes and foot processes (Fig. 4b, c). The morphological changes included irregularities in the width of secondary foot processes of podocytes and changes in the arrangement or unclear margins of each secondary foot process were observed. Elongations of primary foot processes were often observed (Fig. 4c: arrow).

Figure 5 shows Pt-blue-stained glomeruli of steroid-resistant NS specimens that had been diagnosed as FSGS. Most of the glomerular capillary lumina were occluded in these sections. The characteristic findings in FSGS specimens were many round-shaped podocyte cell bodies (Fig. 5a, b: arrows), and an adhesion of glomerular tufts to Bowman's capsule (Fig. 5a: arrowhead). Podocytes and their foot processes were clearly visible at a higher magnification. Figure 5c and 5d shows the parts of other glomeruli from steroid-resistant NS specimens. Protruded and round-shaped podocyte cell bodies and detachments of podocytes from the GBM were also noted. The changes of podocyte foot processes were elongated primary processes and retraction of secondary processes.

In PAM-stained specimens, positively stained GBMs and mesangial matrix of glomeruli were clearly observed under LVSEM in each steroid-sensitive NS (Fig. 6a, c) and steroid-resistant NS (Fig. 6b, d) section. PAM-negative cellular components such as podocytes, endothelial cells, and mesangial cells of glomeruli showed dark appearance, and podocyte foot processes were indistinguishable. LVSEM at a higher magnification allowed detailed investigation of the intact aspects of GBMs through the overlying of other elements by detecting the BSE signals from PAM-positive GBMs of both the subepithelial side and the subendothelial side. Irregularities in thickness and the wrinkling of GBMs were clearly detected in several steroid-resistant NS glomeruli (Fig. 6d), while steroid-sensitive NS GBMs had almost uniform and thinner appearances (Fig. 6c) under LVSEM.

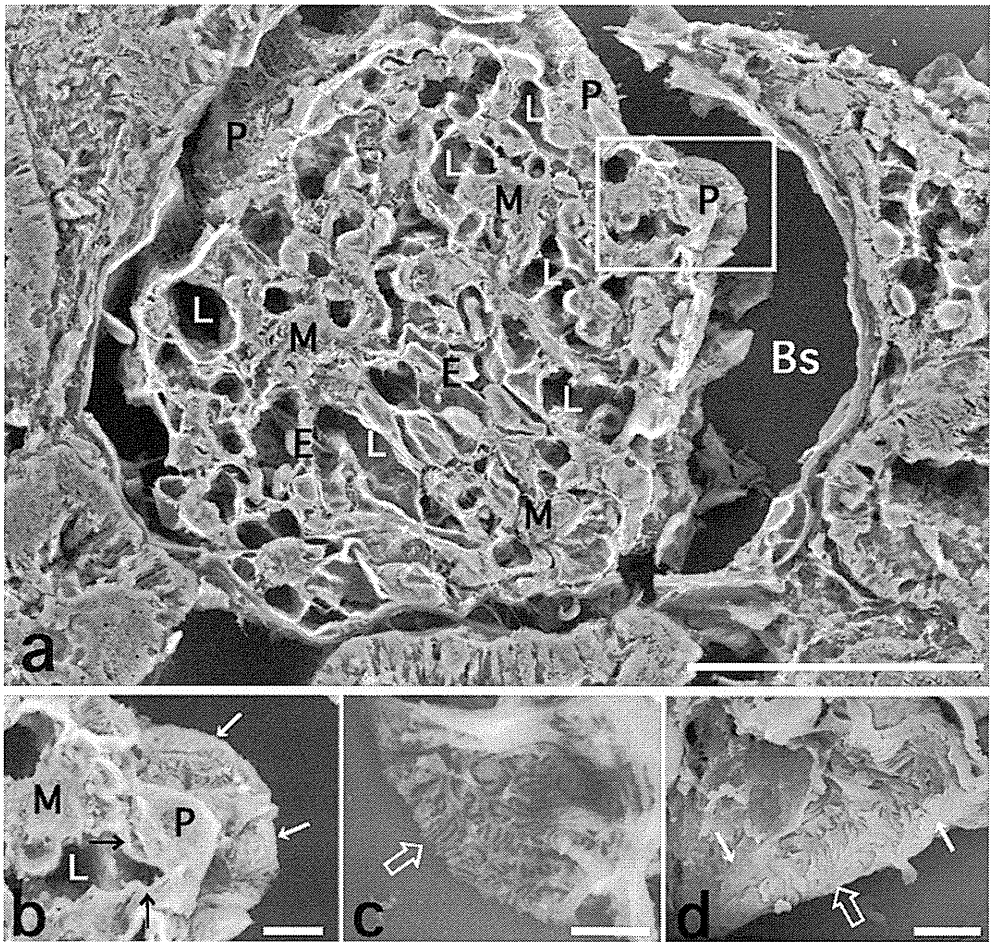

Fig. 3 LVSEM images of Pt-blue-stained glomeruli in steroid-sensitive NS. **a**) Three-dimensional cut surface view of a glomerulus with minor glomerular abnormalities detected by light microscopy. The surface view of the podocytes and their foot processes can be observed from the Bowman's space (Bs). Capillary lumens, endothelial cells and mesangial regions are observable on the cut side view of the glomerulus. **b**) A higher magnification image (×6,000) of the glomerulus within a square shown in (a). Cut surfaces of a podocyte with foot processes (white arrows), a mesangial cell and GBM (black arrows) are discriminated. **c**) High magnification (×10,000) of a part of the glomerulus surface within a square shown in Fig. 2b. Normal alignments of primary and secondary foot processes (open arrow) are observed. **d**) High magnification (×10,000) of a part of another glomerulus in the same case of steroid-sensitive NS is shown. Shortening changes of primary foot processes (white arrows) and an irregular width of a secondary foot process (open arrow) of podocytes are noted. E: endothelial cell, L: capillary lumen, M: mesangial region, P: podocyte. Bars: 50 μm (a), 5 μm (b, c, d)

Figure 7 shows the TEM images obtained from the same biopsy sample shown in Figure 6b and 6d from a steroid-resistant NS patient diagnosed as having FSGS. The fusions, effacements, and flattening of foot processes of podocytes and the detachments of podocytes from the GBM were observed in a glomerular capillary wall segment (×2,500).

DISCUSSION

We used LVSEM for the histological diagnosis of pediatric NS in this study. The novel approach using LVSEM enabled the investigation of three-dimensional structural alterations of glomerular podocytes and GBMs in conventional renal biopsy paraffin sections obtained from pediatric NS patients. The advantages of the present method are that the preparation is very simple and easy, and the differential stainability of glomerular components with Pt-blue or PAM enables the complementary observation of renal biopsy sections under LVSEM with a high resolution close to that of TEM. Because we placed slides with wet sections in the LVSEM chamber, non-dried sections were gradually dried even in the low vacuum condition. Nevertheless, we confirmed that there was no serious deformation of the glom-

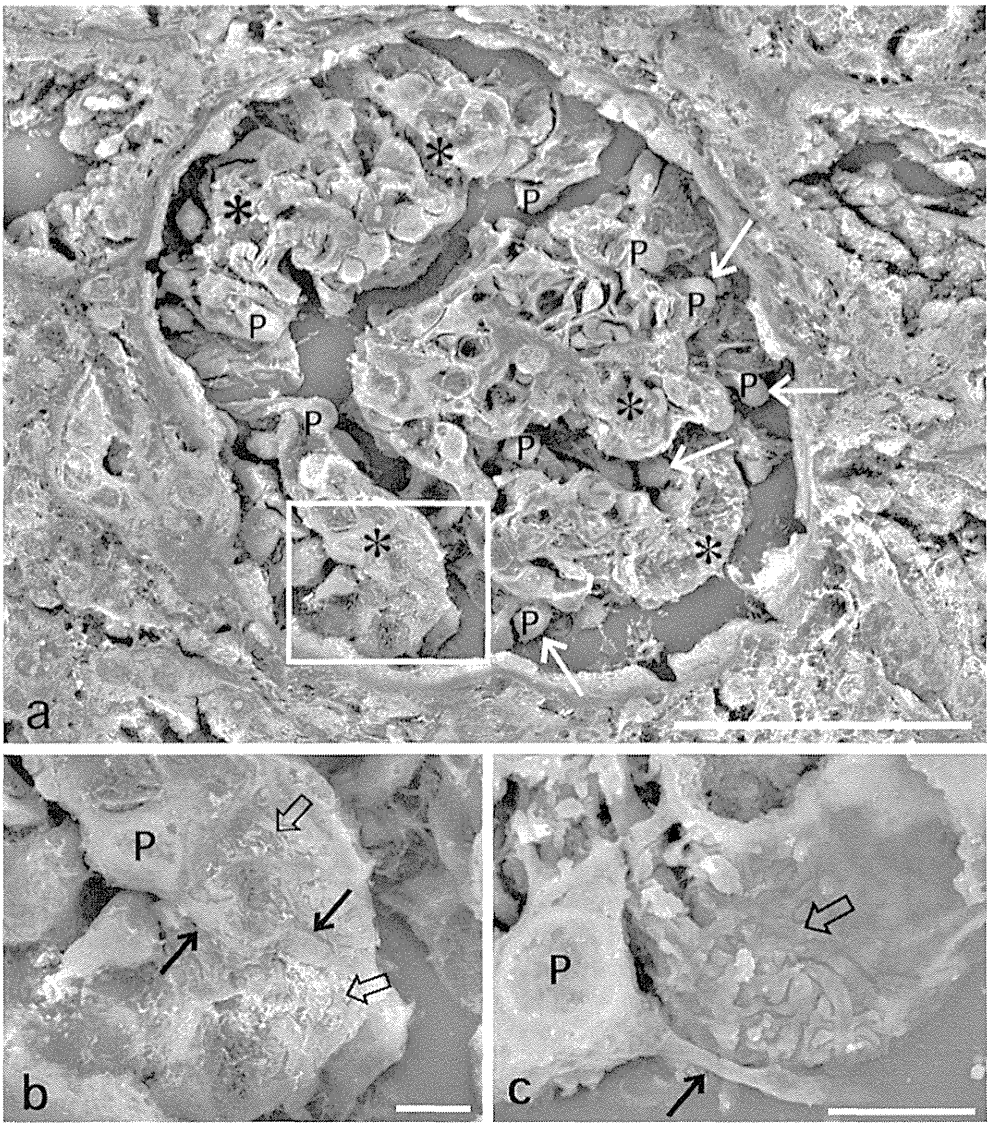

Fig. 4 LVSEM images of Pt-blue-stained glomeruli in steroid-resistant NS. **a**) Surface view of a glomerulus in a paraffin section with minor glomerular abnormalities. The overview of the surface structure of glomeruli can be observed in this specimen, three-dimensionally. Note round-shaped podocyte cell bodies (arrows) and widespread microvillus transformations (asterisks). **b**) Higher-magnification images (×5,000) of glomerular surfaces within a square shown in (a). Secondary foot processes covered with numerous microvilli are not clearly observed (open arrow), although the primary processes (arrows) are barely observed. **c**) A high-magnification image of another glomerulus (×10,000). Elongation of a primary foot process (arrow), irregularities in the width of secondary foot processes, and unclear margins of each secondary foot process were observed (open arrow). P: podocyte. Bars: 50 μm (a), 5 μm (b, c, d)

erulus fine structure in vacuum-dried sections by comparing with freeze-dried sections, even though the slight shrinkage was not avoided (9). Therefore, we observed vacuum-dried specimens without freeze-drying or critical point drying procedure. In fact, Pt-blue-positive cellular elements and PAM-positive GBMs were clearly observed three-dimensionally at an arbitrary magnification between ×50 and ×10,000 under LVSEM.

In the present study, the LVSEM findings of glomeruli differed between the steroid-sensitive NS and steroid-resistant NS specimens, especially in cases with FSGS. At a magnification of ×1,000 under LVSEM, protruding round-shaped podocyte cell bodies were distinctly observed in steroid-resistant NS specimens, although changes of podocyte cell bodies were not conspicuous in steroid-sensitive NS specimens. The three-dimensional recognition of a

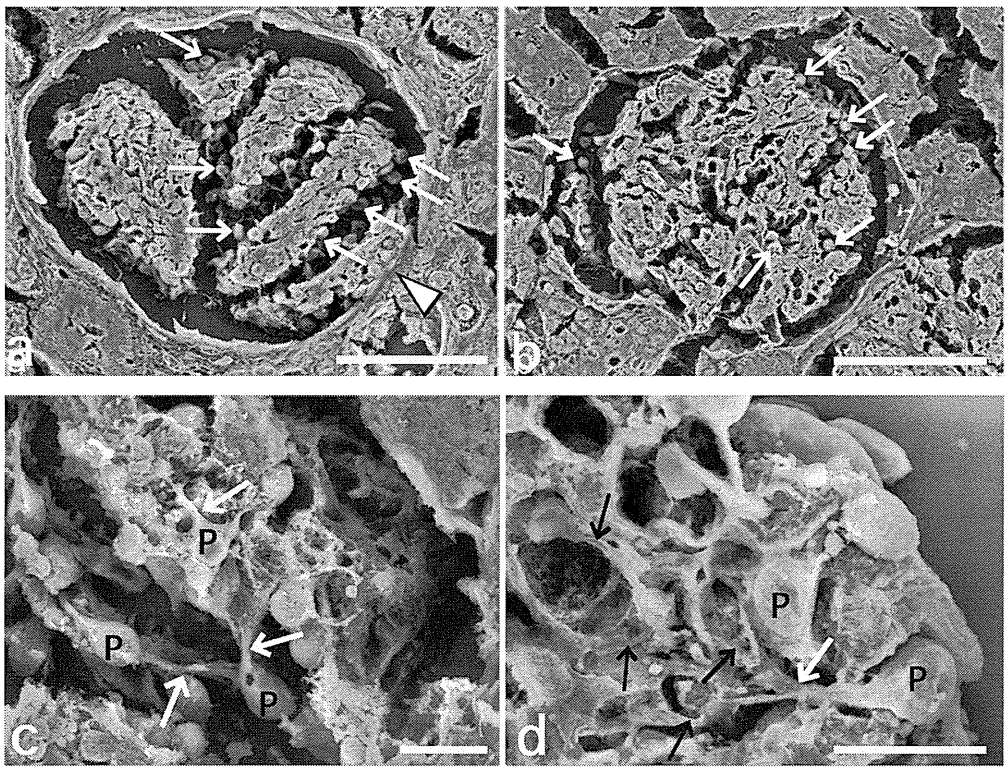

Fig. 5 LVSEM images of Pt-blue-stained glomeruli of steroid-resistant NS specimens that had been diagnosed as FSGS by light microscopy. **a**, **b**) Cut surface views of glomeruli are shown. Most of the glomerular capillary lumina are occluded. Round-shaped podocyte cell bodies are extensively observed (arrows). An adhesion of glomerular tufts to Bowman's capsule (arrowhead) is shown in (a). **c**, **d**) Higher-magnification images (c: ×3,000, d: ×5,000) of other glomeruli are shown. The surface view of podocytes and their foot processes is observed from the Bowman's space. Protruded and round-shaped podocytes and elongations of primary foot processes (white arrows) suggesting detachments of podocyte cell bodies from the GBM (black arrows) are noted. P: podocyte. Bars: 50 μm (a, b), 10 μm (c, d)

wide range of pathological findings of podocytes at a relatively lower magnification is one of the advantages of LVSEM (9). At a higher magnification, various morphological alterations of foot processes of podocytes, so called "foot process effacements or fusions" and "microvillus transformations" were detected in both steroid-sensitive NS and steroid-resistant NS specimens. These findings correspond to the previous TEM findings observed for minor glomerular abnormalities. In addition to these findings, widespread microvillus transformations over most glomerular surfaces, elongations of primary foot processes, and many round-shaped podocytes were protruded under LVSEM in steroid-resistant NS patients diagnosed as having FSGS. It is difficult to discriminate glomeruli with no obvious changes in minor glomerular abnormalities from those with no sclerosis in FSGS using LM. The present LVSEM findings suggest the morphological differences in minor glomerular abnormalities between steroid-sensitive NS and steroid-resistant NS specimens.

Evaluation of the morphological changes of podocytes is important for understanding the pathogenesis of NS. Normal podocytes attached to GBMs have flat-shaped cell bodies. The effaced foot processes of podocytes seen in NS are associated with detachments of the podocytes themselves from the GBM (27). Once the podocytes are damaged for any reason, they become detached from the GBM without recovery. Damaged podocytes have shown morphological changes (18), and therefore, detachment of the damaged podocytes from the GBM may cause the podocyte cell body shape to change to a rounded shape. A uninephrectomy model which leads to FSGS showed enlargement and attenuation of podocyte cell bodies after local detachment of podocytes from the GBM in those areas (18). In the present study, the round-shaped podocyte cell bodies were observed using LVSEM, and the detachment of podocytes from the GBM was observed using TEM. Although our findings of round-shaped podocyte cell bodies seem to be different from those of

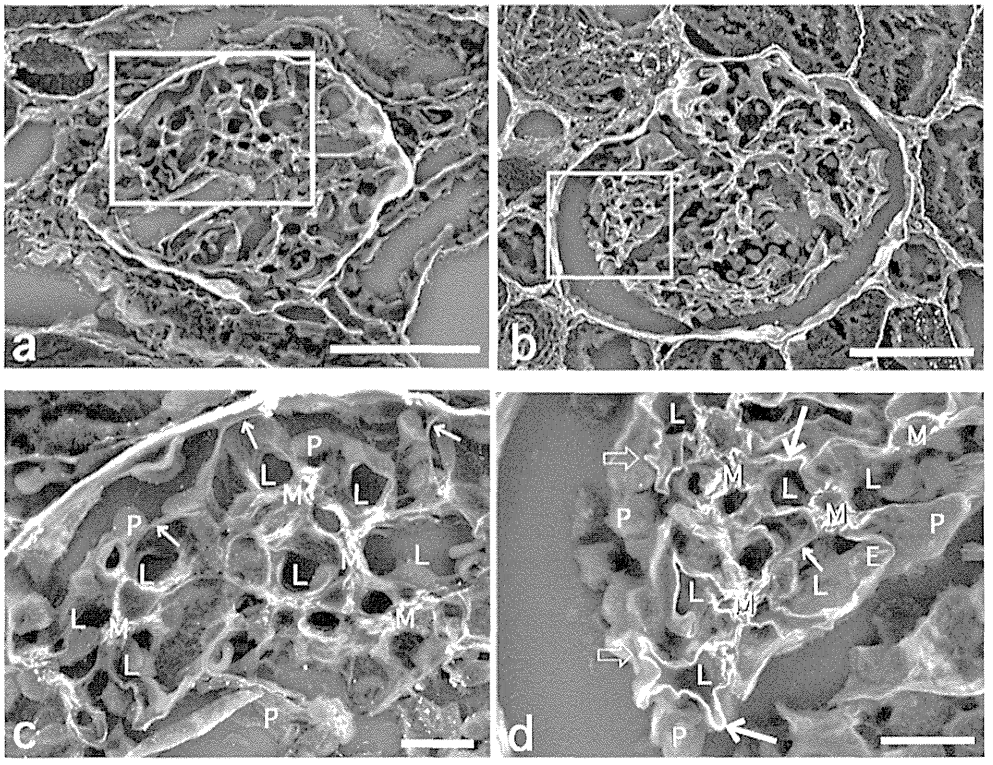

Fig. 6 LVSEM images of PAM-stained glomeruli in steroid-sensitive NS (a, c) and steroid-resistant NS (b, d) specimens. PAM-positive GBM and the mesangial matrix appear bright. In contrast, PAM-negative podocytes and other cells show dark appearances. **c, d**) Higher-magnification images of glomeruli within the square shown in (a) and (b). Almost uniform and thinner GBM (small arrows) is observed in steroid-sensitive NS (c) specimens (×2,500), whereas irregularities in the thickness (small and large arrows) and wrinkling (open arrows) of the GBM are noted in several glomeruli of steroid-resistant NS specimens diagnosed as FSGS (d) (×3,000). L: capillary lumen, M: mesangial matrix, P: podocyte. Bars: 50 μm (a, b), 10 μm (c, d)

podocytes with pseudocysts which was found by using TEM and SEM in previous studies (14–16, 25), our results support the idea that damaged podocytes undergo cell-body morphological changes.

The present results on podocyte alterations observed by LVSEM are also similar to the findings of previous reports. Kuusniemi *et al.* (15) reported pathological findings in congenital NS of the Finnish type (NPHS1), which comprises extreme proteinuria and progresses to end-stage renal disease; SEM revealed protruded podocyte cell bodies with microvillus degeneration, elongated primary processes, and foot process effacement. In puromycin aminonucleoside (PAN) nephrosis, an experimental model of NS in which podocyte injury is caused by PAN administration, severe proteinuria and podocyte foot process effacements develop (27). Kriz *et al.* (14) described the various structural responses of podocytes to stress and injury, focusing on foot process effacement and detachment. In our clinical data, patients with steroid-resistant NS had more intense proteinuria and hypoalbuminemia than patients with steroid-sensitive NS. Accordingly, the present morphological findings determined by LVSEM suggest that many round-shaped podocytes and elongations of primary foot processes are possibly correlated with the clinical states of NS.

Changes in podocyte slit diaphragm proteins are also known to cause proteinuria. Nephrin deficiency leads to NPHS1 with massive proteinuria; podocin, CD2-associated protein, or α-actinin-4 deficiency also leads to proteinuria. Indeed, abnormalities in podocyte slit diaphragm proteins have been found in NS cases (29). Reductions in podocyte slit diaphragm proteins caused morphological changes in podocyte foot processes and result in proteinuria. Furthermore, abnormalities in slit diaphragm proteins in podocyte foot processes caused cytoskeletal changes in podocytes (12). A previous study showed that signals between slit diaphragm proteins have an important role in the regulation of podocyte function, survival, and actin remodeling (3). Morphological changes in the foot processes of podocytes have been correlated with changes in podocyte cell bod-